Prostate megalin is regulated by serum hormone levels and imports globulin-bound testosterone

Jason Garcia[1], Kirsten D. Krieger[1], Candice Loitz[1], Lillian Perez[1,2], Zachary A. Richards[1], Yves Helou[1], Steve Kregel[1], Sasha Celada[1], Clementina A. Mesaros[3,4], Peter H. Gann[1,2], Thomas E. Willnow[5], Donald Vander Griend[1,2], Rick Kittles[6], Gail S. Prins[1,2,7], Trevor Penning[3,4], Larisa Nonn[1,2,*]

[1]Department of Pathology, University of Illinois at Chicago, Chicago, IL 60612, USA
[2]University of Illinois Cancer Center, Chicago, IL 60612, USA
[3]Department of Systems Pharmacology & Translational Therapeutics, University of Pennsylvania Perelman School of Medicine, Philadelphia, PA 19104, USA
[4]Center of Excellence in Environmental Toxicology, Perelman School of Medicine, University of Pennsylvania, Philadelphia, PA 19104, USA
[5]Max-Delbrück- Center for Molecular Medicine, 13125 Berlin, Germany
[6]Department of Population Sciences, City of Hope, Duarte, CA 91010, USA
[7]Departments of Urology, Physiology and Biophysics, University of Illinois at Chicago, Chicago, IL 60612, USA

Correspondence: Larisa Nonn, PhD
Professor of Pathology
840 S. Wood St.
Chicago, IL 60612
312-996-0194
lnonn@uic.edu

Keywords: vitamin D, androgen, prostate cancer, disparities

ABSTRACT

Vitamin D deficiency associates with an increased risk of prostate cancer (PCa) mortality and is hypothesized to contribute to PCa aggressiveness and disparities in African Americans. We previously reported a relationship between African-ancestry, circulating and intraprostatic vitamin D metabolites and prostatic expression of megalin, an endocytic receptor that internalizes globulin-bound hormones. Here, we show prostatic 5α-dihydrotestosterone (DHT) levels are higher in African American men and inversely correlate with serum 25-hydroxyvitamin D (25D) status. We further demonstrate that megalin imports sex hormone-binding globulin-bound testosterone in prostate cells and prostatic loss of *Lrp2* (megalin) results in reduced prostate androgen levels. Megalin expression was suppressed by 25D and DHT in cell lines, patient-derived prostate epithelial cells, and prostate tissue explants, supporting a negative feedback loop. Megalin levels are reduced in localized PCa by Gleason Grade and in patients with future disease recurrence. Our findings highlight the impact of vitamin D deficiency on prostate androgen levels, which are known drivers of PCa, and reveal a potential mechanistic link between vitamin D and the PCa disparities observed in African Americans.

INTRODUCTION

Prostate cancer (PCa) is the second most frequently diagnosed cancer in men in the United States, and African American (AA) men have 60% higher incidence and 200% higher mortality rates than European American (EA) men [1]. The reason for this disparity is multifactorial and involves biological and socioeconomic factors; yet, when controlled for, AA men still present with more aggressive disease. AA men are also at increased risk vitamin D deficiency. The circulating form of vitamin D is 25-hydroxyvitamin D (25D), a steroid hormone essential for normal human physiology and calcium homeostasis [2]. Vitamin D status is dependent on supplementation, sun exposure, and skin pigmentation as melanin reduces UV-induced cutaneous vitamin D synthesis. Vitamin D metabolites exert anti-transformative properties in PCa cells and delay the formation of preneoplastic lesions in a mouse model of PCa [3]. Importantly, circulating levels of 25D are inversely correlated with aggressive PCa [4-9]. Thus, differences in vitamin D are hypothesized to underlie this disparity in PCa in AA men, but the mechanistic pathways remain unclear.

Further, while serum 25D levels are used to assess vitamin D status clinically and in epidemiologic studies, local tissue concentrations of vitamin D metabolites are understudied [10]. Only a small percentage of vitamin D metabolites exist free in circulation, and the majority (88–99%) are bound by vitamin D-binding protein (DBP) or albumin [11]. The free hormone hypothesis suggests that intracellular concentrations of vitamin D metabolites and other hormones are dependent on passive diffusion of hormones not bound by serum globulins [12]. However, we demonstrated that circulating levels of the hormonally active vitamin D metabolite 1,25-dihydroxyvitamin D (1,25D) and prostatic levels of 1,25D do not correlate, indicating that passive diffusion of unbound hormone is not driving 1,25D in the prostate [13]. We also observed difference by ancestry where serum 25D and tissue 1,25D only correlated in white men[13]. Serum DBP also correlated with prostate 25D and 1,25D in white men[13]. 1,25D is the active hormone that binds

the vitamin D receptor (VDR) and 1,25D results from hydroxylation of 25D by cytochrome P450 27B1 (CYP27B1) and it is inactivated by CYP24A1. Because nearly all serum 25D is bound by DBP and albumin, our data support a mechanism by which globulin bound-25D is imported into the prostate and activated to 1,25D by prostatic CYP27B1.

One candidate that may support an active import mechanism is megalin, an endocytic receptor encoded by *LRP2* with a well-characterized function of binding and internalizing DBP-bound 25D from the glomerular filtrate [14,15]. We confirmed that prostate epithelium expresses megalin protein and discovered that prostatic expression of *LRP2* negatively correlated with 25D levels only in AA men[13]. LRP2 also positively correlated with percent West African ancestry in the cohort[13]. These findings suggest that the free hormone hypothesis may not apply in the prostate, and that a compensatory mechanism may increase prostate megalin when systemic levels of 25D are deficient.

Megalin also binds and internalizes sex hormone-binding globulin (SHBG), the serum transporter of testosterone (T). Megalin import of SHBG-bound T occurs most notable in kidney cells, but import of SHBG has also been shown in the LNCaP PCa cells [16]. Circulating T concentrations do not correlate with intraprostatic concentrations, further supporting an alternative to passive diffusion [17]. Megalin-deficient mice exhibit defects in maturation of their reproductive organs, suggesting dysregulation of sex hormones[18]. Polymorphisms in the megalin gene, *LRP2*, associate with PCa recurrence, PCa-specific mortality and the effectiveness of androgen-deprivation therapy (ADT)[19].

We hypothesize that megalin is part of a compensatory mechanism to increase prostatic import of androgen and vitamin D metabolites. This mechanism is highly relevant to PCa disparities since androgens contribute to PCa pathogenesis and AA men are more likely to be 25D deficient. Here, we performed a mechanistic examination of steroid hormone transport by

megalin in prostate cells, patient prostate tissue explants and using mouse model. We further examine hormone and megalin levels in clinical prostate specimens.

RESULTS

Intraprostatic DHT is higher in AA men and inversely correlates with vitamin D status

Our prior study showed that prostate *LRP2* (megalin gene) expression negatively correlated with 25D[13], suggesting that vitamin D deficiency may lead to megalin upregulation and, subsequently, increased prostate import of steroid hormones. To test this hypothesis, we examined the relationships between these hormones in patients. We quantified T and DHT in serum and in benign areas of radical prostatectomy tissue from a cohort of patients with PCa patients for whom we had previously measured vitamin D metabolites [13]. Vitamin D status, as measured by serum 25D level, negatively correlated with intraprostatic DHT (**Figure 1A**) in all patients, but was not significant when analyzed separately by ancestry. AA patients had higher prostate levels of the active hormone DHT (**Figure 1B**) and lower levels of serum T (**Figure 1C**) than EA men. This relationship is consistent with our report on vitamin D metabolites in AA men [13], who had lower serum 25D and higher prostate 1,25D compared to EA men (also shown in **Figure B-C**). The serum and tissue levels of vitamin D metabolites shown here are a subset of the full cohort reported by us in 2017 [13]. Dehydroepiandrosterone (DHEA), a precursor to T and DHT, was also measured in the sera and was undetectable. DHT was the predominant androgen in the prostate with T levels were undetectable in the majority of patients (data not shown), supporting metabolism to DHT once in the tissue. Conversely, T was the most abundant in the serum with DHT levels 2 orders of magnitude lower than serum T and did not differ by ancestry (data not shown). Overall, the inverse correlation of serum 25D with intraprostatic DHT supports our hypothesis that serum vitamin D deficiency and low serum T are drivers of higher prostatic DHT levels.

Prostate cells express megalin and import SHBG-bound T

Megalin transcript (*LRP2*) and protein expression were compared between prostate cells. Both gene and protein were detected in benign primary patient-derived prostate epithelial cells (PrE AA1 and PrE AA2), immortalized benign prostate epithelial cells (957E-hTERT), and in PCa cell lines (LNCaP, 22Rv1) (**Figure 2A,B**). All cell types express the vitamin D receptor (VDR), however, benign PrE cells (AA1, AA2 and 957E-hTERT) lack androgen receptor (AR) expression (**Figure 2A**). PCa cells (LNCaP and 22Rv1) have low to no expression of CYP27B1 (**Figure 2A**), and are unable to metabolize 25D to the active hormone, 1,25D, as shown by lack of CYP24A1 induction (**Figure S1**). LNCaP and 22Rv1 PCa cell lines were used to examine androgen import (T) and AR activity in vitro as they have differential expression of megalin and express AR. When treated with T alone and SHBG-T, both LNCaP and 22Rv1 cells showed AR activation, as evidenced by increased *KLK3* mRNA (**Figure 2C**). SHBG was added at 20-fold excess and incubated with T for 30 min before treating cells to ensure thorough hormone-globulin binding. To inhibit megalin, cells were pre-incubated with receptor-associated protein (MEG-Inh)[20](**Figure 2C**). Both LNCAP and 22Rv1 cells exhibited decreased *KLK3* gene expression and ARE luciferase when cells were pretreated with MEG-Inh before hormone treatments; however, the magnitude of inhibition was higher in 22Rv1 cells, which express more megalin. Pre-incubation with MEG-Inh did not block the response of added T alone, demonstrating specific to SHBG-T and not T (**Figure S2**). To visualize SHBG-T internalization, we used Alexa Fluor 555-labeled human SHBG (SHBG-555). SHBG-555 localized to the plasma membrane of LNCaP and 22Rv1 cells in response to SHBG and SHBG + T treatment (**Figure 2D**). Addition of SHBG-T showed more internalization and punctate patterns than SHBG treatment alone, and MEG-Inh blocked the internalization of SHBG. These data demonstrate that SHBG-bound T is available to prostate cells in a megalin-dependent manner.

Knockout of *Lrp2* in mouse prostate reduces T

To determine if prostate T levels are affected by the absence of megalin, we created a prostate-specific knockout of *Lrp2,* since the obligate *Lrp2* knockout causes perinatal lethality in most affected animals [21,22]. Tamoxifen (TAM)-inducible prostate-specific knockout of *Lrp2* was generated by crossing an *Lrp2*-floxed mouse[23] (a gift from Dr. Willnow) with the probasin-driven TAM-inducible Cre recombinase mouse (Pb-MerCreMer)[24] (**Figure 3A**). We encountered no breeding problems with the homozygous bitransgenic line. *Lrp2*$^{fl/fl}$/*Cre*$^{+/+}$ mice and control (*Lrp2*$^{fl/fl}$ only and *Cre*$^{+/+}$ only) mice were injected with TAM at postnatal day 10 (P10-TAM), which resulted in recombination of the genomic DNA in only the prostate and not in mouse tails (**Figure 3B**). Day 10 injections were stopped due to complications with injecting young pups, and subsequent injections were at 5 weeks. Prostates, testes, and sera were collected at 24 and 32 weeks of age for androgen measurement by liquid chromatography–tandem mass spectrometry (LC–MS/MS). There were no significant differences in prostate hormones between P10-TAM and 5W-TAM animals. Prostate T and DHT levels were significantly lower in *Lrp2*$^{fl/fl}$/*Cre*$^{+/+}$ mice than in control mice, (**Figure 3C**). Serum T and testes T levels were tightly correlated in all mice, supporting testes as the source of serum T. However, neither prostate T nor DHT significantly correlated to serum T in control and *Lrp2*$^{fl/fl}$/*Cre*$^{+/+}$ mice (**Figure 3D**), suggesting that prostate T levels are not due to passive diffusion from the serum. In addition, prostate T and DHT only significantly correlated in the control *Lrp2*$^{fl/fl}$ only, suggesting regulation of T to DHT is different in the prostates lacking *Lrp2*. Serum DHT was undetectable in most mice. Although the differences in the prostate androgens were significant, there were no differences in prostate histology, prostate weight, and fertility (data not shown). Relationships between serum and tissue hormone levels support a regulated transport mechanism of T into the prostate, rather than passive diffusion of serum T.

Vitamin D and androgen negatively regulate *LRP2* expression

The inverse relationship between vitamin D status, as measured by serum 25D, and prostate DHT (**Figure 1**), combined with our previous finding of a negative correlation between serum 25D and *LRP2* expression in AA men , suggest negative regulation of *LRP2* by vitamin D. Therefore, we sought to characterize the impact of vitamin D on *LRP2* expression in vitro. Primary prostate epithelial cells (PrE-AA1) treated with 10 nM 25D exhibited decreased *LRP2* expression (**Figure 4A**). Because our results showed that SHBG-T was imported into PCa cells (**Figure 2**), we also examined regulation of *LRP2* by T and observed a similar suppressive effect (**Figure 4A**).

To assess the regulation of *LRP2* expression at the transcriptional level, we characterized *LRP2* promoter activity in vitro. The VDR forms an obligate heterodimer with retinoid X receptor (RXR) and binds to vitamin D response elements (VDREs). Analysis of this *LRP2* promoter fragment identified multiple RXR:VDR and AR motifs (**Figure 4B**; **Figure S3**). The *LRP2* promoter was cloned into a *Renilla* luciferase reporter plasmid (*LRP2-Rluc*), which was suppressed in 957E-hTERT cells by 25D and in 22Rv1 cells by T (**Figure 4C**). 957E-hTERT cells are advantageous for luciferase experiments because they can be transfected at a high efficiency. Further, 957E-hTERT cells are benign epithelial prostate cells that do not express AR and are similar to PrE cells in phenotype. These transcriptional analyses support the hypothesis that *LRP2* expression is regulated by hormone-stimulated transcription factors in response to 25D and T.

PrE and 957E cells respond to 25D but do not express AR. Conversely, 22Rv1 cells do not have active CYP27B1 to bioactivate 25D. Thus, we examined these responses in fresh ex vivo benign human prostate tissue slice cultures (**Figure 4D**), which express all components of androgen and vitamin D activation/response pathways, including *CYP27B1* (vitamin D 25-hydroxylase), *VDR*, *LRP2*, and *SRD5A* (T to DHT conversion), and *AR* (data not shown). Hormone responsiveness was demonstrated by robust induction of *CYP24A1* and *KLK3* gene expression by 25D and T, respectively, alone or in the presence of their serum-binding globulins, DBP and SHBG (**Figure S4A**)**.** Megalin protein and *LRP2* expression were decreased in tissue slices treated with 25D alone or T (**Figures 4E-F**), consistent with our observation in cell lines

and the relationships we previously observed between serum 25D and prostate *LRP2* in patient data[13]. Examination of murine prostate epithelial *Lrp2* gene expression in publicly available single-cell RNA-sequencing data showed upregulation after castration and downregulation following regeneration with T [25](**Figure 4G**). These findings strongly support vitamin D-mediated negative-feedback on *LRP2* expression and identify a second feedback loop regulated by androgens.

Megalin and *LRP2* levels are lower in PCa

A tissue microarray (TMA) composed of prostate cores from 29 patients (20 AA, 9 EA) with four cores from each patient, two benign and two PCa regions per patient, was stained for megalin. Fluorescence intensity was digitally quantified in epithelial regions using the epithelial marker Pan-CK to segment the epithelium (**Figure 5A**). Frozen tissues were not available for patients represented in this TMA; therefore, we could not correlate tissue hormone levels with megalin expression. Megalin protein levels were significantly lower in PCa areas than in benign tissues (**Figure 5A**). The majority of the PCa on this TMA was Gleason 3, with only 5 cases of Gleason 4 and no difference by Gleason was observed in this small cohort. *LRP2* expression was assessed in larger cohorts using publically available data sets. Analyses of gene expression data from a Dana Farber cohort of localized PCa[26] showed that LRP2 levels decrease with primary Gleason grade (**Figure 5B left panel**) and are lower in patients who had future biochemical recurrence (BCR) (**Figure 5B right panel**). In a cohort of castration resistant tumors, PCa *LRP2* levels were highest in men with lowest PSA in a cohort of 63 men[27] (**Figure 5C**), supporting regulation by androgens. Together, the PCa data support that *LRP2* expression is highest in tissue that are normal and most differentiated, which is consistent with localization of megalin to the luminal cells.

DISCUSSION

This study follows our recent finding that megalin protein is expressed in the membrane of prostate epithelium and that megalin gene expression correlates with vitamin D status and percentage of African ancestry[13]. These findings led us to hypothesize that megalin is part of a compensatory pathway to increase intraprostatic vitamin D metabolites when patients are deficient. As polymorphism in LRP2 associate with PCa aggressiveness and response to ADT[19], here we focus on how this increase in megalin would also increase import of SHBG-bound T, which is also known to be imported by megalin. We show that megalin imports SHBG-bound T, is regulated by T and vitamin D, and is dysregulated in PCa. These findings provide a direct link between vitamin D deficiency and the disparity of PCa in AA men.

The presence of a compensatory feedback loop to regulate intraprostatic hormones levels has implications for the AA population who are disproportionately vitamin D deficient [28]. In our cohort, serum 25D and prostatic DHT were significantly inversely correlated, consistent with vitamin D regulation of hormone import via megalin. Moreover, AA men had higher levels of DHT in prostate tissue than EA men and lower levels of serum T, further supporting active transport of SHBG-T rather than passive diffusion of T. The tight correlation of prostate and serum levels of vitamin D metabolites and androgen metabolites suggests co-regulation. Further, elevated prostatic DHT may directly contribute to the increased incidence of aggressive PCa and PCa mortality among AA men as lower prostate androgens has been shown to decrease the risk of PCa and PCa mortality[29-31]. This relationship outlines an intricate yet detrimental interaction between androgen and vitamin D axes that characterizes the adverse effects of a double disparity in men of West African descent.

Our serum finding that serum T is lower in AA men differs from prior studies that found no racial differences in serum total T or free T [32,33]. This discrepancy may reflect differential assay and sample preservation methods. Although our results were significant, we acknowledge that

there is a limitation of under-representation of vitamin D-replete AA patients and vitamin D-deficient EA patients in the cohort, which is needed to separate ancestry from deficiency.

We examined megalin as a mediator of prostate androgen levels as our prior study showed its expression to be positively correlated to West African ancestry and inversely correlated to serum vitamin D status[13]. Seventy percent of circulating T is bound to SHBG [16] with about 5% free T and the remaining bound to albumin. T is thought to follow the free hormone hypothesis, with only free or albumin-bound T available to tissues. We show that megalin binds and internalizes SHBG-bound T, which is similar to other reports in LNCaP cells [16]. This occurred in PCa cell lines and fresh prostate tissue slices, which internalized SHBG-bound T resulting in *KLK3* induction. We further demonstrated that loss of megalin in mouse prostate epithelium decreased prostate levels of androgens. Although knockout mice demonstrate some regulation of prostate T by megalin, it is important to note that mice differ from humans in that mice primarily circulate albumin-bound T rather than SHBG-T. However, megalin is a multiligand recepter and also mediates albumin uptake [34]. Our findings do not rule out the presence of other SHBG-T uptake receptors [35]. The data shown here support megalin-dependent import of SHBG-T into the prostate and are consistent with full *Lrp2* knockout[18], which displays impaired descent of the testes into the scrotum and other defects consistent with sex steroid disruption.

A negative feedback loop was previously reported for vitamin D skeletal myotube cultures in which growth in high levels of 25D significantly decreased DBP-bound 25D uptake in cultures [36]. We similarly observed that high levels of 25D decreased the expression of *LRP2* and megalin protein. T also negatively regulated megalin, demonstrating interplay between hormones, likely to tightly control the intracellular levels of steroids. This was also observed in vivo in mouse prostates following castration and regeneration with exogenous androgens. These findings also support the need to avoid vitamin D deficiency in PCa patients being treated with anti-androgen therapies. However, our findings to present a bit of a paradox in that *LRP2* expression is regulated

by the extracellular amounts of hormones, yet we observed higher levels of androgens and vitamin D metabolites within the prostates from AA men. It was unexpected that the serum levels of hormones correlate with *LRP2* expression rather that the tissue levels. These findings reveal the complexities of endocrine hormone regulation within tissues and suggest there is an intermediary sensor not yet described.

Given the dependence of PCa on androgens and the prior report of LRP2 polymorphisms with PCa aggressiveness[19], we examined megalin protein and *LRP2* gene expression in multiple cohorts of PCa patients. Megalin protein was markedly lower in cancer tissue than in benign tissue in radical prostatectomy samples. In publically available cohorts, *LRP2* gene expression further decreased by Gleason, suggesting its expression is connected to differentiated cells. We also found the patients who had BCR had lower *LRP2*, which is likely connected to its relationship to Gleason. These findings suggest that PCa may be less dependent on megalin and utilize free hormones once it is established. On the other hand, we did see that PSA levels inversely correlated with *LRP2* in a cohort of castrate resistant PCa, supporting that it may still be regulated by androgens in these tumors.

The interplay between vitamin D status, megalin, and cancer may also extend to breast cancer, another hormone-responsive disease. For example, HME-immortalized breast epithelial cells and T47D breast cancer cells are able to internalize DBP-bound 25D and activate *CYP24A1* [37]. Additional work shows that SHBG binds circulating estradiol and, as of 2016, AA women are nearly 1.5 times more likely to develop lethal triple-negative breast cancer than white women [38]. These studies show that megalin-mediated endocytosis of globulin-bound hormones extends to breast tissue and could perhaps outline a double disparity that contributes to increased breast cancer mortality in AA women.

An important consideration regarding race-related differences is that race is a social construct and a proxy for ancestry. We are not suggesting that there are biological differences by

a patient's self-declared race. Rather, because vitamin D status is directly correlated to skin pigmentation, our findings suggest that vitamin D supplementation may reduce the levels of prostate androgens, which would mostly affect AA men who tend to be vitamin D deficient.

In conclusion, our in vitro and ex vivo data show that megalin is functional in the prostate and responsible for transporting protein-bound hormones into the cell, which complicates the free hormone hypothesis. We also show that megalin expression is negatively regulated by vitamin D, and, in times of deficiency, megalin is upregulated, potentially increasing import of both vitamin D and T. This may signify a once-protective compensatory mechanism of vitamin D gone awry, increasing the likelihood of androgen import and increasing the probability of harmful androgen actions that may contribute to the disparity in PCa aggressiveness that plagues AA men.

METHODS

Patient sera and prostate tissue

De-identified fresh-frozen prostate and sera were collected from radical prostatectomy patients under IRB exemption (IRB 2018-0281). Specimens from 60 patients were included for analysis: 30 from the UIC Hospital (Chicago, Illinois, USA) and 30 from the Cooperative Human Tissue Network (CHTN) Western Division at Vanderbilt University (Nashville, Tennessee, USA). Criteria for inclusion were self-declared race data, >500 mg of benign frozen prostatectomy specimen, and availability of sera. All patients had localized PCa without prior chemotherapy or hormone therapy. Samples were obtained from two deidentified biorepositories: CHTN and UIC. Because samples were deidentified, the research was determined to not fit the definition of human subjects research by the UIC IRB (2013-0341).

Hormone measurement in patient samples

Calibration curve. Standard compounds T and DHT and internal standard (IS) d3T were purchased from Cerilliant (Round Rock, TX, USA). Nine calibrators (0.0625, 0.125, 0.25, 0.5, 1,

5, 10, 50, and 100 ng/mL in methanol) were used to establish calibration curves with spiked-in IS. Curves were fitted by linear regression with a weighting factor of 1/*x*. *Sample preparation and extraction.* Tissue samples and ISs were mixed and bead homogenized using a Mikro-Dismembrator II (Handelskontor Freitag, Germany) before extraction. The extraction took place three times with hexane:ethyl acetate (60:40 [vol:vol]). The organic layer from each extraction was collected, combined, and dried under nitrogen. The residue was reconstituted in methanol:water (20:80 [vol:vol]) and subjected to solid-phase extraction using an ISOLUTE C18 SPE cartridge (100 mg, 1 mL) following the manufacturer's protocol. The final eluate was dried before for LC–MS analysis. Human serum samples were extracted by the same procedure.

LC–MS/MS analysis. Quantification of T and DHT was achieved using an SCIEX Qtrap 6500 spectrometer coupled with an Agilent 1290 ultra performance liquid chromatography (UPLC) system. Dried sample was reconstituted in methanol and resolved by a Waters ACQUITY UPLC BEH C18 column (1.7 μm, 2.1 × 100 mm) maintained at 45° at a flow rate of 450 μL/min. Elution started with 60% of mobile phase A (5% methanol in water, 0.1% formic acid), followed by a linear gradient increase of mobile phase B (acetonitrile with 0.1% formic acid) from 40 to 80%. MS data were acquired by multiple reaction monitoring (MRM) in positive mode with an electrospray ionization (ESI) source voltage at 5.0 kV and temperature at 450°C. T, DHT, and D3T were detected by monitoring their transitions to signature product ions 289>97 (T), 291>255 (DHT), and 292>97 (D3T), respectively. Data were analyzed using Analyst software. *Vitamin D metabolite measurement.* Extraction and measurement of 25D was performed as previously reported by our group [13].

Cell lines

HEK293, LNCaP, and 22Rv1 cells were purchased from ATCC (VA, USA), and 957E-hTERT cells were generously donated by John Isaacs and maintained in keratinocyte serum-free medium (KSFM) (ThermoFisher Scientific). PrE-AA1 and PrE-AA2 cells are primary patient-derived

epithelial cells derived in our lab by previously reported methods [39,40]. HEK293 cells were maintained in Dulbecco's Modified Eagle's medium (DMEM) (Gibco) supplemented with 10% (vol/vol) fetal bovine serum (FBS) (Gibco). LNCaP and 22Rv1 cells were maintained in phenol-free Roswell Park Memorial Institute (RPMI) (Gibco) medium supplemented with 10% (vol/vol) FBS. Cells were switched to 5% (vol/vol) charcoal-stripped FBS (Millipore-Sigma) overnight and serum starved for 1 h before experimentation. Primary prostate cells established from fresh male radical prostatectomy tissues were isolated as previously described and cultured in prostate cell growth medium (Lonza). All cells were cultured at 37°C with 5% CO_2. All cells are described in **Table S1**.

RNA isolation and reverse transcription–quantitative PCR (RT–qPCR)

RNA was isolated by the Trizol method (ThermoFisher Scientific). RNA concentration and quality were determined by measuring the absorbance ratio at 260/280 nm using a NanoDrop One spectrophotometer (ThermoFisher Scientific). Total RNA (500 ng) was reverse transcribed using the high-cCapacity cDNA reverse transcription kit (Applied Biosystems). Resulting cDNA was used for quantitative PCR amplification on a QuantStudio6 machine (ThermoFisher Scientific) using gene-specific primers (**Table S2**) and FastStart Universal SYBR Green master mix (Millipore-Sigma). Reactions were run in duplicate, and relative C_t values were normalized and calculated independently using the $-\Delta\Delta C_t$ method to the expression of the housekeeping genes *HPRT1* and *RPL13A* (all primers are listed in **Table S1**).

Western blotting

Cells were grown to 80% confluency, and protein lysates were collected in cell lysis buffer (9803, Cell Signaling Technology). Protein (30 µg) was run on a Bis-Tris protein gel (NuPAGE) and transferred to a PVDF membrane. Membranes were blocked for 1 h using Odyssey Blocking Buffer (LiCOR) and probed with anti-megalin rabbit monoclonal antibody (1:1,000; M02463,

Boster Bio) and anti-actin (1:1,000; 4499S, Cell Signaling Technology) and with secondary antibodies against rabbit and mouse (926-68071, LiCOR). Blots were imaged using the Odyssey CLx imaging system (LiCOR).

T and SHBG treatments

LNCAP and 22Rv1 cells at 80% confluency were incubated with 25 nM T ± 125 nM human SHBG (SHBG-8259H, Creative BioMart) and 1 μM receptor-associated protein (MEG-Inh) (BML-SE552-0100, Enzo Life Sciences) for 16 h. T and SHBG were preincubated for 30 min before addition to cells. Cells were pretreated with megalin inhibitor for 1 h before hormone addition.

Luciferase reporter assays

Cells at 70% confluency were transfected with luciferase plasmids, and luciferase activity was measured after 48 h using the dual-luciferase reporter assay system and GloMax 20/20 (Promega). pRL-null *Renilla* plasmid was cotransfected at 0.4 pg/μL to control for transfection efficiency. For *LRP2* promoter, 0.2 ng/μL *LRP2* promoter-driven *Renilla* luciferase reporter (S712992, Switchgear Genomics) and 0.4 pg/μL PGL4.50 *Photinus pyralis* (E310, Promega) luciferase reporter were simultaneously treated with 10 nM 25D or 10 nM T. *Renilla* luciferase relative light units are defined as the ratio of *Renilla* to *Photinus* activity.

DBP-488 and SHBG-555 internalization

Recombinant human SHBG (ProSpec, Israel) was directly labeled with Alexa Fluor-555 using protein conjugation kit (ThermoFisher Scientific) according to the manufacturer-supplied protocol. Aliquots of globulin conjugate were stored at −20°C until use. Cells were grown to 70% confluency in eight-well chamber slides and incubated with SHBG-555 alone, SHBG-555 +T, or MEG-Inh + SHBG-555 + T as described above. After 4 h, cells were counterstained with Alexa Fluor 647 Phalloidin (F-actin) and DAPI (ThermoFisher Scientific) and visualized by confocal microscopy.

Lrp2-flox/Pb-MerCreMer mice

The University of Illinois at Chicago Office of Animal Care and Institutional Biosafety (OACIB) approved all procedures involving animals in this study. Transgenic mice harboring the probasin promoter driving MerCreMer were acquired from The Jackson Laboratory (ProbasinBAC-MerCreMer or C57BL/6-Tg(Pbsn-cre/Esr1*)14Abch/J, strain 020287). Generation of mice with *loxP* sites flanking *Lrp2* exons 71 through 75 ($Lrp2^{fl/fl}$) was previously described [21]. $Lrp2^{fl/fl}$ mice were crossbred with Pb-MerCreMer homozygous ($cre^{+/+}$) mice. F1 cross progeny were mated to generate $Lrp2^{fl/fl}/cre^{+/+}$ mice. Mice were genotyped by Transnetyx and injected with TAM (50 mg/kg) at two stages of development (P10 or 5 weeks). Control TAM-injected mice were $Lrp2^{fl/fl}$ or $cre^{+/+}$. To confirm recombination, DNA was isolated from tail snips and prostate cell pellets using a DNeasy Blood & Tissue kit (Qiagen) followed by PCR with DreamTaq Green PCR master mix (ThermoFisher Scientific) using primers spanning exons 71–75 and primers spanning exons 76–77 as a control. PCR products were imaged on agarose gels. All mouse primers are listed in **Table S2**.

Mouse DHT and T quantitation

A protocol similar to that described by Higashi et al. was followed [41]. Briefly, the internal standard mix (500 pg each of T-IS, DHT-IS, E1-IS, and E2-IS and 100 pg of 3α- and 3β-diol) were added to 0.6 mL of 0.1 mM PBS in a homogenization vial kept in ice. Frozen tissue (around 20 mg of tissue) was cut on a tile in dry ice with a blade kept in dry ice and added directly to the homogenization vial. The tissue was homogenized two times for 10 min in ice in a Bullet Blender. The homogenate was moved to a borosilicate tube, and ethyl ether (4 mL) was added and shaken for 30 min, followed by incubation for 2 h at 50°C with shaking at 4°C overnight. The sample was then centrifuged at 1,500*g* for 10 min. Using a glass pipette, the upper organic phase was

transferred into a new borosilicate tube. The organic phase was dried under nitrogen. Samples were stored at −20°C before derivatization and LC–MS analysis, as previously described .

Ex vivo prostate tissue slice culture

Fresh prostate tissue was acquired from radical prostatectomy patients from UIC with informed consent (IRB 2007-0694). Tissue from a 5-mm punch was sliced into 300-µm sections using an Alabama Tissue Slicer (Alabama Research and Development), placed on titanium alloy inserts within a six-well plate, and maintained in 2.5 mL of KSFM supplemented with 5% (vol/vol) charcoal-stripped FBS and 50 nM R1881 (PerkinElmer) [42]. Slices were cultured overnight, rotating at a 30° angle at 37°C with 5% CO_2. Alternate slices were collected for RNA extraction and formalin fixation. For gene expression, RNA isolation and RT–qPCR was performed as described above. Only slices with confirmed benign epithelial content (high expression of KRT8 and undetectable *PCA3* by RT–qPCR) were included in the analyses.

Immunohistochemistry

Formalin-fixed paraffin-embedded slices were sectioned to 5 µm, deparaffinized, processed for steam antigen retrieval (10 mM sodium citrate, 0.05% Tween 20, pH 6), and stained with anti-megalin (1:500; ab76969, Abcam) overnight at 4°C. A rabbit secondary antibody HRP/DAB kit was used to visualize with hematoxylin counterstain (ab64261, Abcam)

TMA immunostaining and analysis

The TMA contained 118 prostate biopsy cores from 29 patients (20 AA, 9 EA) and consisted of at least two benign and cancer cores from each patient. A board-certified pathologist reviewed each core to confirm cancer grade mark regions for exclusion if they contained artifacts or benign areas intermixed with cancer. Sections (5 µm) were incubated with rabbit polyclonal anti-megalin (ab76969) diluted 1:100 and mouse monoclonal anti-panCK (AE1/AE3) diluted 1:2,000, followed

by incubation with secondary antibody Alexa Fluor 488 goat anti-rabbit diluted 1:200 and Alexa Fluor 555 goat anti-mouse diluted 1:200 (Life Technologies, Carlsbad, CA, USA) and counterstaining with DAPI. Sections were scanned at ×20 on a Vectra3 multispectral imaging system (Akoya Biosciences, Marlborough, MA). Epithelial areas were identified and segmented by machine learning using the panCK marker and HALO software (Indica Labs, Albuquerque, NM) and adjusted manually to ensure accuracy. Epithelial megalin fluorescence intensity was quantified and reported as average intensity per pixel of the segmented area of each core using Inform software. A Mann–Whitney unpaired U test was used to compare benign cores to PCa cores for all men, EA only, and AA only.

LRP2 expression in public datasets

PCa tumor and metastases RNA-sequencing datasets were previously reported and described by our group. *LRP2* expression was analyzed by analysis of variance (ANOVA) with Kruskal–Wallis for multiple comparisons. Mouse prostate single-cell RNA sequencing was from Karthaus et al. using data from the epithelial cluster from three mice per timepoint intact, 1, 7, and 28 days after castration, and 1, 7, and 28 days after adding back T to regenerate the prostate [25]. *Lrp2* expression was extracted from the Broad Single Cell Portal.

Statistics

Statistical analysis methods used in each experiment are detailed within the figure legends and methods.

Data availability

All data generated or analyzed during this study are included in this published article (and its supplementary information files).

DECLARATION OF INTEREST

There is no conflict of interest that could be perceived as prejudicing the impartiality of the research reported.

AUTHOR CONTRIBUTIONS

J.G., K.D.K., C.L., L.P., S.C., Z.A.R. and S.K. conducted the experiments. Y.H. maintained the mouse colony. C.A.M. conducted hormone quantitation. T.E.W. provided the *Lrp2*flox mouse model and edited the manuscript. P.H.G. and D.V.G. provided TMA and patient datasets, respectively, and edited the manuscript. G.S.P, R.K., T.P., and L.N. secured funding. J.G., L.P., and L.N. wrote the manuscript.

FUNDING

This research was funded by the Department of Defense Prostate Cancer Research Program Idea Award for Disparities Research PC170484 (L.N., T.P., R.K., and G.S.P.) and NIH awards 1R21CA231610-01 (L.N.) and P30-ES013508 (C.A.M. and T.P.).

ACKNOWLEDGEMENTS

Tissue samples were provided by the UI Health Biorepository and the CHTN, an NCI-supported resource. We thank Klara Valyi-Nagy and Alexandru Cristian Susma from the UI Health Biorepository, Ryan Deaton and the UIC research Histology and Tissue Imaging Core for assistance with the tissue microarray analysis, Vicky Macias and Andre Kajdacsy-Balla for assessment of pathology of patient tissues, Morgan Zenner and Michael Schlicht for assistance with generating tissues slices, and Hui Chen for editing the methods. Finally, we thank the patient participants and Drs. Michael Abern, Daniel Moreira, and Simone Crivellaro for procurement of radical prostatectomy tissue specimens.

FIGURE LEGENDS

Figure 1. Ancestry-specific differences in androgen levels and relationships between DHT and 25D. (A) Correlation between serum 25D and prostate DHT in EA (n = 29) and AA (n = 28) men measured by uHPLC-MS-MS. Correlation values (r) were determined using Spearman's rank test. (B) Prostate tissue levels of 1,25D and DHT (C) and serum 25D and T levels measured by uHPLC-MS-MS. Graphs represent mean with 95% confidence interval (95% CI). The P values were determined by unpaired two-tailed t test.

Figure 2. Prostate cells express megalin and import SHBG-bound T. (A) Gene expression of *LRP2, AR, VDR* and *CYP29B1* in a panel of prostate cell lines as shown by RT–qPCR shown as relative quantitation to *HPRT*. Error bars are standard error of the mean (SEM). (B) western blot for megalin in prostate cell line panel. (C) Regulation of *KLK3* (prostate-specific antigen [PSA] gene) expression after 24 h following treatment with vehicle control (CTL), 50 nM T alone (T), 50 nM T preincubated with 500 nM SHBG (SHBG), or T + SHBG in cells preincubated with 1μM MEG-Inh in LNCaP and 22Rv1 PCa lines. (D) Visualization (×63) of SHBG-555 (red) import into cells with DAPI (blue) nuclear and F-actin (green) cytoskeletal counterstains. Statistical analysis was performed using a one-way ANOVA with a two-stage linear step-up procedure of Benjamini, Krieger, and Yekutieli for multiple comparisons; *P < 0.05 for comparison to CTL, ^P < 0.05 for comparison to T + SHBG. All graphs represent mean ± SEM of three or more individual experiments with two replicates per experiment.

Figure 3. Loss of *Lrp2* in mouse prostate reduces prostatic androgens. (A) Mouse model for conditional knockout of *Lrp2* in prostate epithelium. (B) Recombination of *Lrp2* exons 71–75 after TAM treatment in prostate DNA (P) but not in tail DNA (T) only in bitransgenic mice. PCR for exons 76–77 was performed as a positive control. (C) prostate levels of T and DHT quantified by LC–MS/MS for $Lrp2^{fl/fl}$ and $Lrp2^{fl/fl}/cre^{+/+}$. Graphs show mean with maximum–minimum bars. (D)

Heat map of Pearson correlation coefficients (*R*) for tissue and serum androgens for P10-TAM mice (*Lrp2*$^{fl/fl}$ n=5, *Lrp2*$^{fl/fl}$/*cre*$^{+/+}$n=6). The *P* value is shown within each cell; NS, not significant.

Figure 4. Negative regulation of *LRP2* and megalin protein by vitamin D and T in cells and tissue slice explants. (A) *LRP2* expression following 24 h of treatment with 50 nM 25D or T in PrE-AA1 or 22Rv1 cells, respectively. (B) *LRP2* promoter contains RXR:VDR- and AR-binding motifs. (C) Activity of a custom *LRP2* promoter luciferase construct after 24 h of 50 nM 25D or T treatment in 975E-hTERT or 22rv1 cells; RLU, relative luciferase units normalized to transfection control. (D) Ex vivo prostate tissue slice workflow. (E) RT–qPCR analysis of *LRP2* expression in prostate tissue slices after 16 h of treatment with 50 nM 25D or T. Relative gene expression is shown as relative quantity (RQ) normalized to *RPL13A*; CTL, vehicle control for all experiments. (F) Images and quantiation of megalin protein expression by IHC in tissue slices after 24 h of treatment with 50 nM 25D or T. Scale bar = 150 μm. The graph shows the mean pathologist score per gland. Graphs show mean ± SEM from triplicate repeats. For tissue slices, graphs show representative experiment mean ± standard deviation (SD) with two replicates per experiment. *P* values were determined using an unpaired *t* test (A, B, and E) or by Kruskal–Wallis and Dunn's multiple comparison tests to CTL (F); $^{*}P < 0.01$. (G) scRNAseq expression of mouse lrp2 in prostate epithelial cells from prostates during a cycle of castration and regeneration from Karthaus et al[25].

Figure 5. Megalin expression is dysregulated in cancer. (A) Digital quantitation of epithelial megalin expression on a TMA consisting of 118 prostate biopsy cores from 29 patients (EA, *n* = 9; AA, *n* = 20). Epithelial regions were segmented by panCK staining, and benign and cancer regions were determined by a board-certified pathologist. Scale bar = 100 μm. Immunofluorescence (IF) intensity per pixel for megalin expressed as mean ± SEM; Ben, benign. (B) *LRP2* expression in RNAseq data set of primary PCa tumors by primary Gleason grade and

future BCR from Gerhauser et al[26] . Analyses by Gleason was ANOVA with post test for linear trend and unpaired t test between Gleason 3 and 4 or 5 combined. BCR *P* values were determined by a Mann–Whitney test. *$P < 0.01$.**$P<0.001$ (C) *LRP2* expression in RNAseq data set of castration resistant PCa tumors by serum PSA from Kumar et al[27]. ANOVA followed by post test for linear trend.

REFERENCES

1 Siegel, R. L., Miller, K. D. & Jemal, A. Cancer statistics, 2018. *CA Cancer J Clin* **68**, 7-30, doi:10.3322/caac.21442 (2018).

2 Abern, M. R. *et al.* Race is associated with discontinuation of active surveillance of low-risk prostate cancer: results from the Duke Prostate Center. *Prostate Cancer Prostatic Dis* **16**, 85-90, doi:10.1038/pcan.2012.38 (2013).

3 Banach-Petrosky, W. *et al.* Vitamin D inhibits the formation of prostatic intraepithelial neoplasia in Nkx3.1;Pten mutant mice. *Clinical cancer research : an official journal of the American Association for Cancer Research* **12**, 5895-5901, doi:10.1158/1078-0432.CCR-06-1039 (2006).

4 Steck, S. E. *et al.* Association between Plasma 25-Hydroxyvitamin D, Ancestry and Aggressive Prostate Cancer among African Americans and European Americans in PCaP. *PLoS One* **10**, e0125151, doi:10.1371/journal.pone.0125151 (2015).

5 Shui, I. M. *et al.* Circulating vitamin D, vitamin D-related genetic variation, and risk of fatal prostate cancer in the National Cancer Institute Breast and Prostate Cancer Cohort Consortium. *Cancer* **121**, 1949-1956, doi:10.1002/cncr.29320 (2015).

6 Nyame, Y. A. *et al.* Associations Between Serum Vitamin D and Adverse Pathology in Men Undergoing Radical Prostatectomy. *J Clin Oncol* **34**, 1345-1349, doi:10.1200/JCO.2015.65.1463 (2016).

7 Murphy, A. B. *et al.* Vitamin D deficiency predicts prostate biopsy outcomes. *Clin Cancer Res* **20**, 2289-2299, doi:10.1158/1078-0432.CCR-13-3085 (2014).

8 Feldman, D., Krishnan, A. V., Swami, S., Giovannucci, E. & Feldman, B. J. The role of vitamin D in reducing cancer risk and progression. *Nat Rev Cancer* **14**, 342-357, doi:10.1038/nrc3691 (2014).

9 Christakos, S., Dhawan, P., Verstuyf, A., Verlinden, L. & Carmeliet, G. Vitamin D: Metabolism, Molecular Mechanism of Action, and Pleiotropic Effects. *Physiol Rev* **96**, 365-408, doi:10.1152/physrev.00014.2015 (2016).

10 Chun, R. F. *et al.* Vitamin D and DBP: the free hormone hypothesis revisited. *The Journal of steroid biochemistry and molecular biology* **144 Pt A**, 132-137, doi:10.1016/j.jsbmb.2013.09.012 (2014).

11 Cooke, N. E. & Haddad, J. G. Vitamin D binding protein (Gc-globulin). *Endocr Rev* **10**, 294-307, doi:10.1210/edrv-10-3-294 (1989).

12 Mendel, C. M. The free hormone hypothesis: a physiologically based mathematical model. *Endocr Rev* **10**, 232-274, doi:10.1210/edrv-10-3-232 (1989).

13 Richards, Z. *et al.* Prostatic compensation of the vitamin D axis in African American men. *JCI insight* **2**, e91054-e91054, doi:10.1172/jci.insight.91054 (2017).

14 Christensen, E. I., Birn, H., Storm, T., Weyer, K. & Nielsen, R. Endocytic receptors in the renal proximal tubule. *Physiology (Bethesda)* **27**, 223-236, doi:10.1152/physiol.00022.2012 (2012).

15 Nykjaer, A. *et al.* An endocytic pathway essential for renal uptake and activation of the steroid 25-(OH) vitamin D3. *Cell* **96**, 507-515 (1999).

16 Li, H. *et al.* Sex Hormone Binding Globulin Modifies Testosterone Action and Metabolism in Prostate Cancer Cells. *Int J Endocrinol* **2016**, 6437585, doi:10.1155/2016/6437585 (2016).

17 Cook, M. B. *et al.* Relationships between Circulating and Intraprostatic Sex Steroid Hormone Concentrations. *Cancer Epidemiol Biomarkers Prev* **26**, 1660-1666, doi:10.1158/1055-9965.EPI-17-0215 (2017).

18 Hammes, A. *et al.* Role of endocytosis in cellular uptake of sex steroids. *Cell* **122**, 751-762, doi:10.1016/j.cell.2005.06.032 (2005).

19 Holt, S. K. *et al.* Association of megalin genetic polymorphisms with prostate cancer risk and prognosis. *Clin Cancer Res* **14**, 3823-3831, doi:10.1158/1078-0432.CCR-07-4566 (2008).

20 Sengul, S., Erturk, S., Khan, A. M. & Batuman, V. Receptor-associated protein blocks internalization and cytotoxicity of myeloma light chain in cultured human proximal tubular cells. *PLoS One* **8**, e70276, doi:10.1371/journal.pone.0070276 (2013).

21 Leheste, J. R. *et al.* Megalin knockout mice as an animal model of low molecular weight proteinuria. *Am J Pathol* **155**, 1361-1370, doi:10.1016/S0002-9440(10)65238-8 (1999).

22 Willnow, T. E. *et al.* Defective forebrain development in mice lacking gp330/megalin. *Proc Natl Acad Sci U S A* **93**, 8460-8464, doi:10.1073/pnas.93.16.8460 (1996).

23 Bachmann, S. *et al.* Kidney-specific inactivation of the megalin gene impairs trafficking of renal inorganic sodium phosphate cotransporter (NaPi-IIa). *J Am Soc Nephrol* **15**, 892-900, doi:10.1097/01.asn.0000120389.09938.21 (2004).

24 Birbach, A., Casanova, E. & Schmid, J. A. A Probasin-MerCreMer BAC allows inducible recombination in the mouse prostate. *Genesis* **47**, 757-764, doi:10.1002/dvg.20558 (2009).

25 Karthaus, W. R. *et al.* Regenerative potential of prostate luminal cells revealed by single-cell analysis. *Science* **368**, 497-505, doi:10.1126/science.aay0267 (2020).

26 Gerhauser, C. *et al.* Molecular Evolution of Early-Onset Prostate Cancer Identifies Molecular Risk Markers and Clinical Trajectories. *Cancer Cell* **34**, 996-1011 e1018, doi:10.1016/j.ccell.2018.10.016 (2018).

27 Kumar, A. *et al.* Substantial interindividual and limited intraindividual genomic diversity among tumors from men with metastatic prostate cancer. *Nat Med* **22**, 369-378, doi:10.1038/nm.4053 (2016).

28 Forrest, K. Y. & Stuhldreher, W. L. Prevalence and correlates of vitamin D deficiency in US adults. *Nutr Res* **31**, 48-54, doi:10.1016/j.nutres.2010.12.001 (2011).

29 Goodman, P. J. *et al.* Long-Term Effects of Finasteride on Prostate Cancer Mortality. *N Engl J Med* **380**, 393-394, doi:10.1056/NEJMc1809961 (2019).

30 Grubb, R. L. *et al.* The REDUCE Follow-Up Study: low rate of new prostate cancer diagnoses observed during a 2-year, observational, followup study of men who participated in the REDUCE trial. *J Urol* **189**, 871-877, doi:10.1016/j.juro.2012.09.099 (2013).

31 Redman, M. W. *et al.* Finasteride does not increase the risk of high-grade prostate cancer: a bias-adjusted modeling approach. *Cancer prevention research* **1**, 174-181, doi:10.1158/1940-6207.CAPR-08-0092 (2008).

32 Mohler, J. L. *et al.* Racial differences in prostate androgen levels in men with clinically localized prostate cancer. *J Urol* **171**, 2277-2280 (2004).

33 Richard, A. *et al.* Racial variation in sex steroid hormone concentration in black and white men: a meta-analysis. *Andrology* **2**, 428-435, doi:10.1111/j.2047-2927.2014.00206.x (2014).

34 Zhai, X. Y. *et al.* Cubilin- and megalin-mediated uptake of albumin in cultured proximal tubule cells of opossum kidney. *Kidney Int* **58**, 1523-1533, doi:10.1046/j.1523-1755.2000.00314.x (2000).

35 Rosner, W., Hryb, D. J., Kahn, S. M., Nakhla, A. M. & Romas, N. A. Interactions of sex hormone-binding globulin with target cells. *Mol Cell Endocrinol* **316**, 79-85, doi:10.1016/j.mce.2009.08.009 (2010).

36 Abboud, M. *et al.* 1,25-Dihydroxycholecalciferol (calcitriol) modifies uptake and release of 25-hydroxycholecalciferol in skeletal muscle cells in culture. *J Steroid Biochem Mol Biol* **177**, 109-115, doi:10.1016/j.jsbmb.2017.10.018 (2018).

37 Rowling, M. J., Kemmis, C. M., Taffany, D. A. & Welsh, J. Megalin-mediated endocytosis of vitamin D binding protein correlates with 25-hydroxycholecalciferol actions in human mammary cells. *J Nutr* **136**, 2754-2759 (2006).

38 Howlader N, N. A., Krapcho M, Miller D, Brest A, Yu M, Ruhl J, Tatalovich Z, Mariotto A, Lewis DR, Chen HS, Feuer EJ, Cronin KA. *SEER Cancer Statistics Review, 1975-2016*, <https://seer.cancer.gov/csr/1975_2016/> (2018).

39 Giangreco, A. A. *et al.* Tumor suppressor microRNAs, miR-100 and -125b, are regulated by 1,25-dihydroxyvitamin D in primary prostate cells and in patient tissue. *Cancer prevention research* **6**, 483-494, doi:10.1158/1940-6207.CAPR-12-0253 (2013).

40 Nonn, L., Peng, L., Feldman, D. & Peehl, D. M. Inhibition of p38 by vitamin D reduces interleukin-6 production in normal prostate cells via mitogen-activated protein kinase phosphatase 5: implications for prostate cancer prevention by vitamin D. *Cancer research* **66**, 4516-4524, doi:10.1158/0008-5472.CAN-05-3796 (2006).

41 Higashi, T. *et al.* Determination of prostatic androgens in 10 mg of tissue using liquid chromatography-tandem mass spectrometry with charged derivatization. *Anal Bioanal Chem* **382**, 1035-1043, doi:10.1007/s00216-005-3233-1 (2005).

42 Maund, S. L., Nolley, R. & Peehl, D. M. Optimization and comprehensive characterization of a faithful tissue culture model of the benign and malignant human prostate. *Lab Invest* **94**, 208-221, doi:10.1038/labinvest.2013.141 (2014).

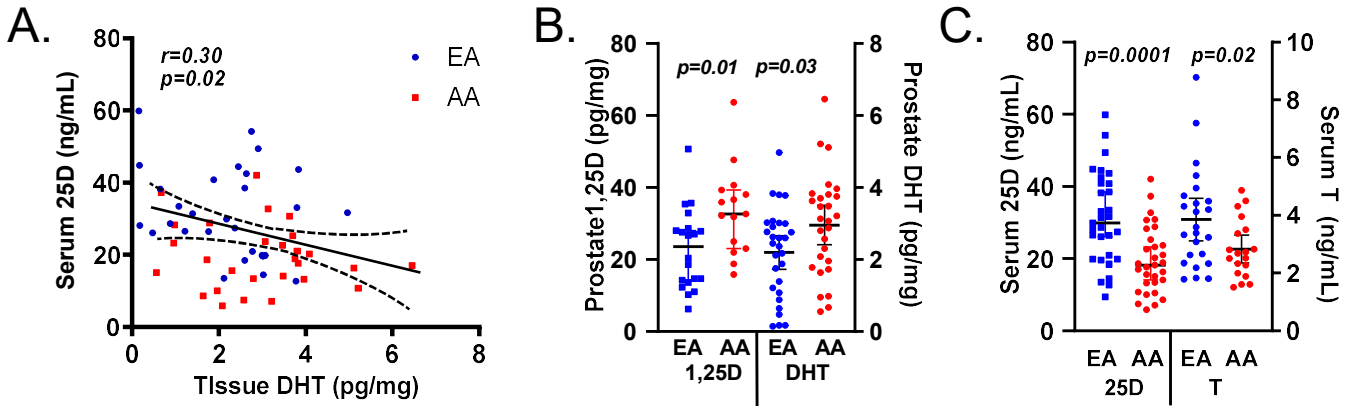
A.
r=0.30
p=0.02
EA
AA
Serum 25D (ng/mL)
TIssue DHT (pg/mg)
B.
p=0.01
p=0.03
Prostate1,25D (pg/mg)
Prostate DHT (pg/mg)
EA AA
1,25D
EA AA
DHT
C.
p=0.0001
p=0.02
Serum 25D (ng/mL)
Serum T (ng/mL)
EA AA
25D
EA AA
T

Figure 1

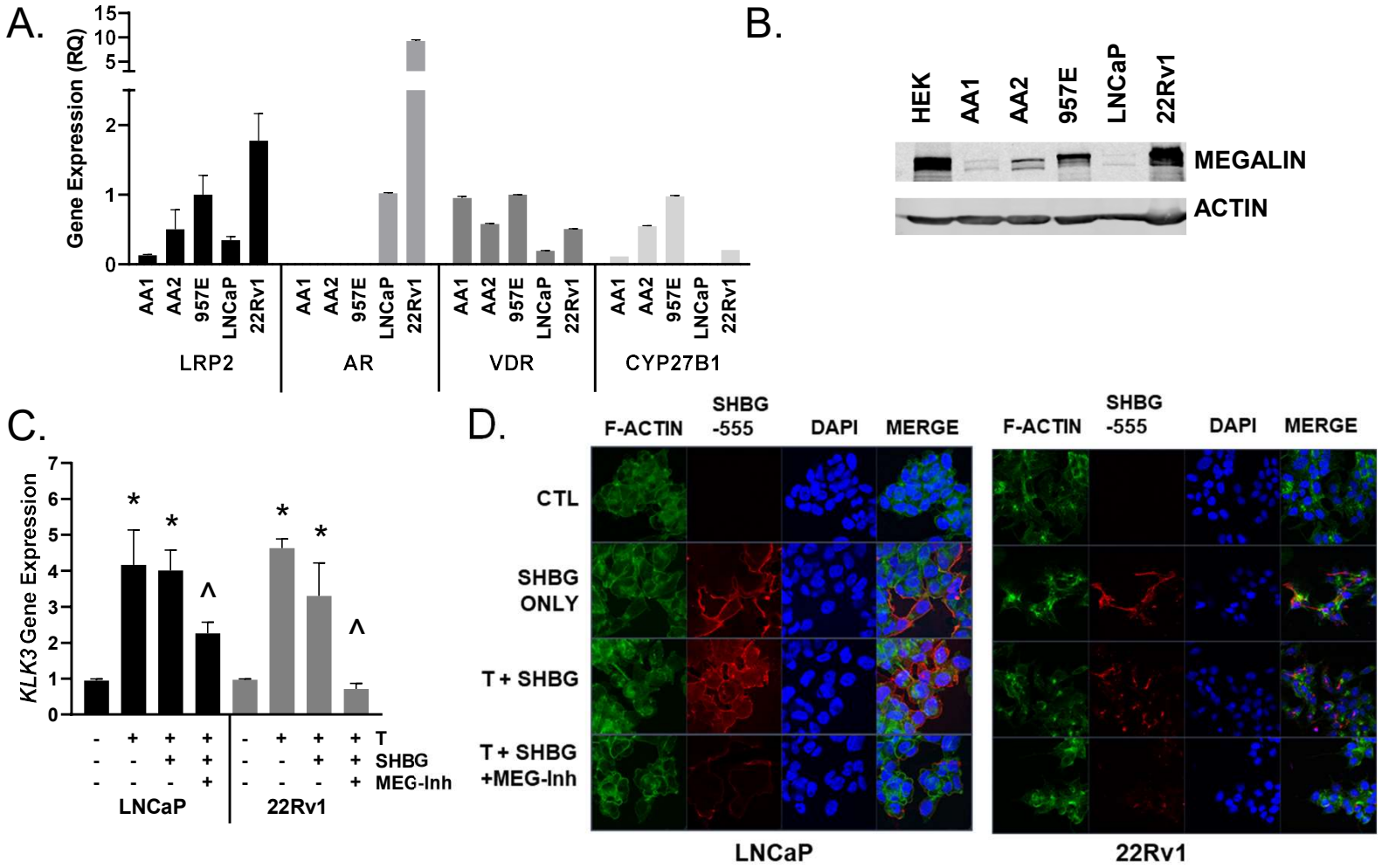
A.
Gene Expression (RQ)
15
10
5
2
1
0
AA1
AA2
957E
LNCaP
22Rv1
LRP2
AR
VDR
CYP27B1
B.
HEK
AA1
AA2
957E
LNCaP
22Rv1
MEGALIN
ACTIN
C.
KLK3 Gene Expression
7
6
5
4
3
2
1
0
*
^
T
SHBG
MEG-Inh
LNCaP
22Rv1
D.
F-ACTIN
SHBG -555
DAPI
MERGE
CTL
SHBG ONLY
T + SHBG
T + SHBG +MEG-Inh
LNCaP
22Rv1

Figure 2

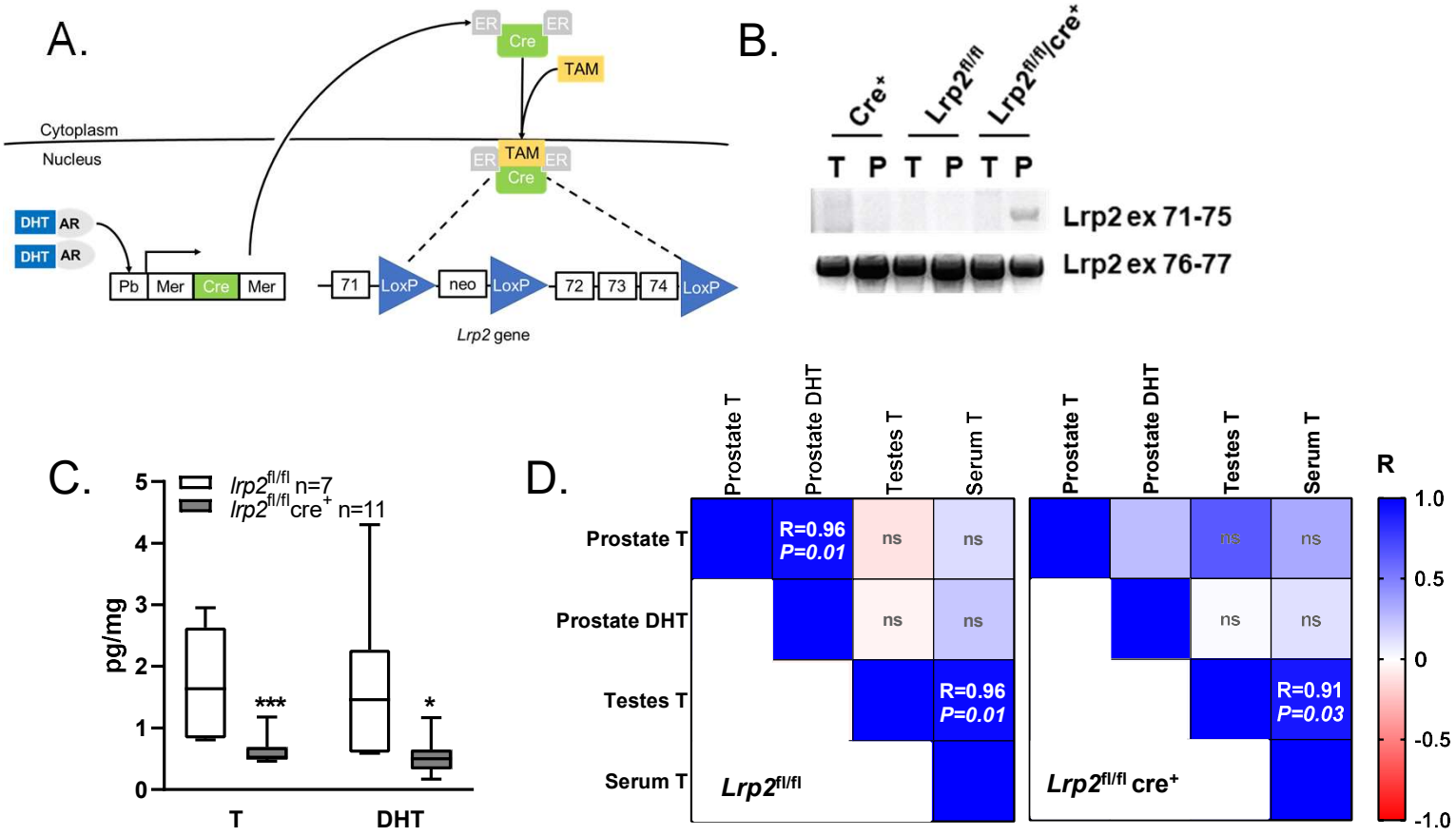
A.
ER
Cre
ER
TAM
Cytoplasm
Nucleus
ER
TAM
ER
Cre
DHT
AR
DHT
AR
Pb
Mer
Cre
Mer
71
LoxP
neo
LoxP
72
73
74
LoxP
Lrp2 gene
B.
Cre+
Lrp2fl/fl
Lrp2fl/fl/cre+
T P T P T P
Lrp2 ex 71-75
Lrp2 ex 76-77
C.
lrp2fl/fl n=7
lrp2fl/flcre+ n=11
pg/mg
5
4
3
2
1
0
***
*
T
DHT
D.
Prostate T
Prostate DHT
Testes T
Serum T
R=0.96
P=0.01
ns
ns
ns
ns
R=0.96
P=0.01
Lrp2fl/fl
Prostate T
Prostate DHT
Testes T
Serum T
ns
ns
ns
ns
R=0.91
P=0.03
Lrp2fl/fl cre+
R
1.0
0.5
0
-0.5
-1.0

Figure 3

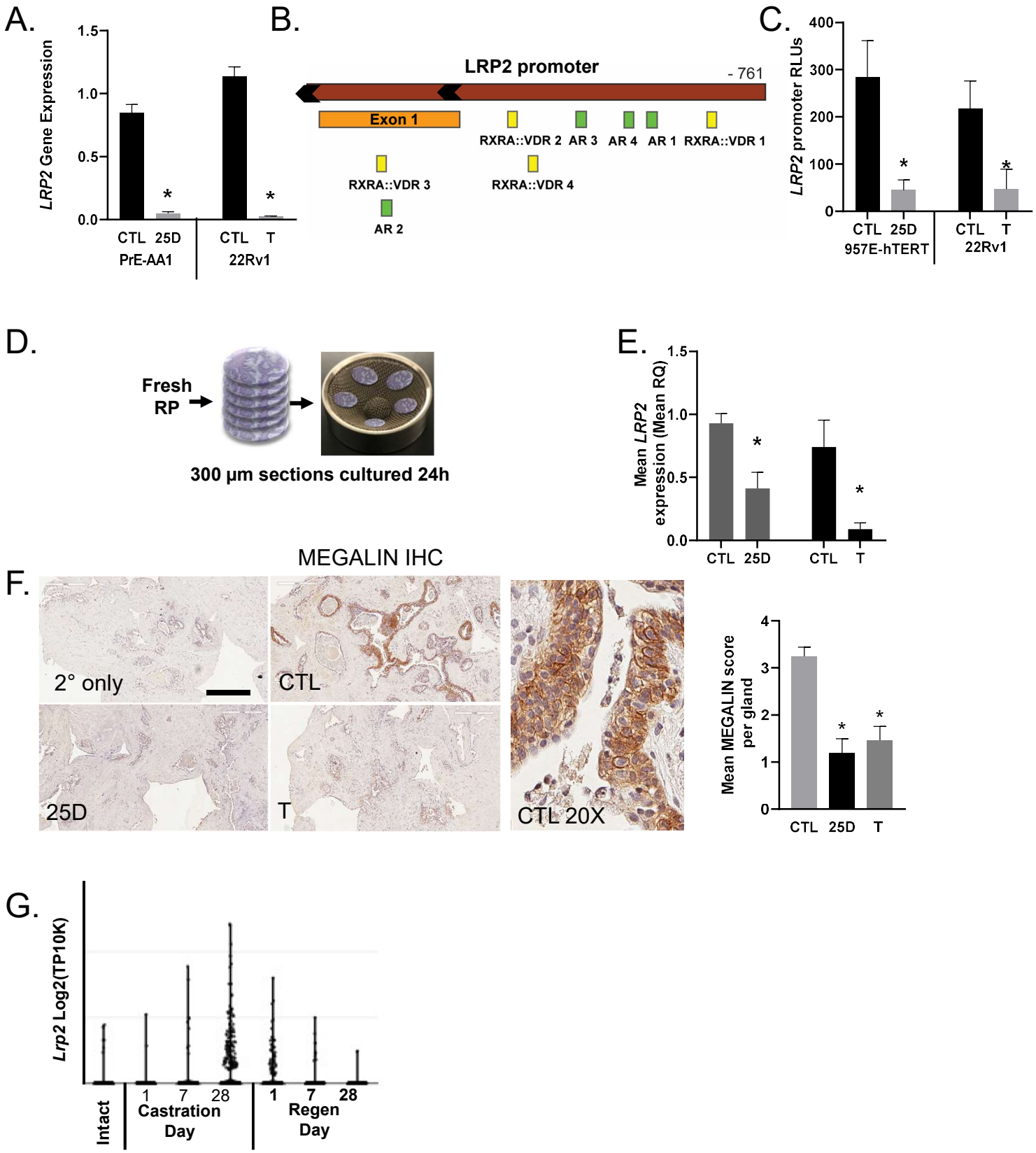
A.
LRP2 Gene Expression
1.5
1.0
0.5
0.0
CTL 25D
PrE-AA1
CTL T
22Rv1
B.
LRP2 promoter
- 761
Exon 1
RXRA::VDR 2
AR 3
AR 4
AR 1
RXRA::VDR 1
RXRA::VDR 3
RXRA::VDR 4
AR 2
C.
LRP2 promoter RLUs
400
300
200
100
0
CTL 25D
957E-hTERT
CTL T
22Rv1
D.
Fresh RP
300 µm sections cultured 24h
E.
Mean LRP2 expression (Mean RQ)
1.5
1.0
0.5
0.0
CTL 25D
CTL T
F.
MEGALIN IHC
2° only
CTL
25D
T
CTL 20X
Mean MEGALIN score per gland
4
3
2
1
0
CTL 25D T
G.
Lrp2 Log2(TP10K)
Intact
1 7 28
Castration Day
1 7 28
Regen Day

Figure 4

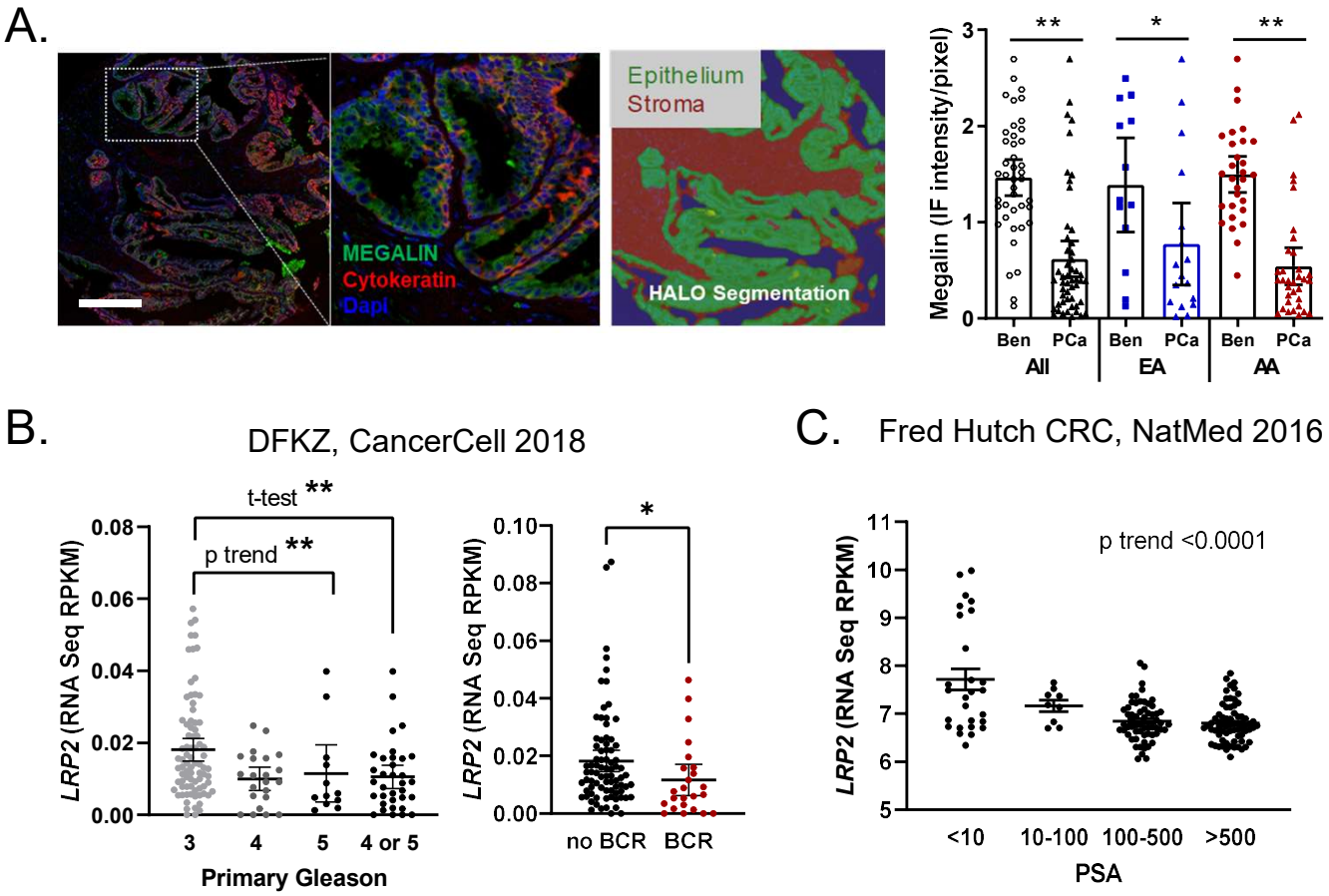
A.
MEGALIN
Cytokeratin
Dapi
Epithelium
Stroma
HALO Segmentation
Megalin (IF intensity/pixel)
Ben
PCa
All
EA
AA
B.
DFKZ, CancerCell 2018
t-test **
p trend **
LRP2 (RNA Seq RPKM)
3
4
5
4 or 5
Primary Gleason
no BCR
BCR
C.
Fred Hutch CRC, NatMed 2016
p trend <0.0001
<10
10-100
100-500
>500
PSA

Figure 5

Supplemental Figures

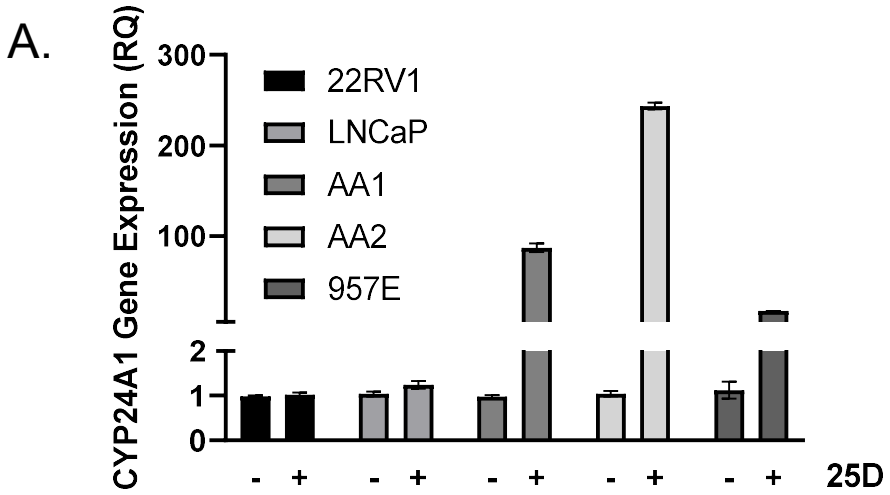

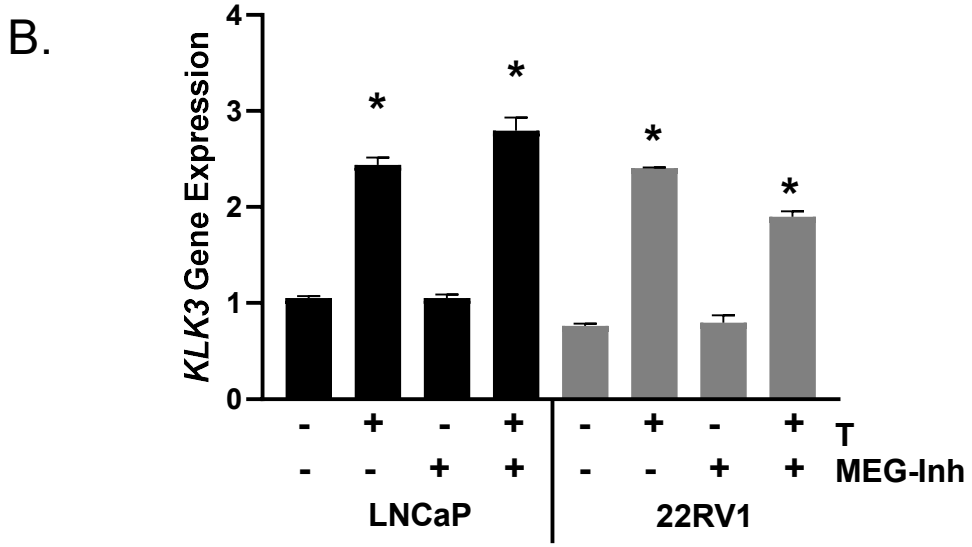

Figure S1. Accompanies Figure 2. A, PCa cells lines do not respond to 25D**.** RT-qPCR for *CYP24A1* following 16 hours of 50 nM 25D treatment in serum free conditions. **B**, Megalin inhibitor does not impact activity and import of T alone. RT-qPCR for *KLK3* following 16 hours of 10 nM T treatment. Cells were pretreated with 1 μM MEG-inhibitor for 1 hour before T. Expression shown as relative quantitation to *HRPT*. Error bars are SEM. *p<0.01

A.

5'CCTGTATCCTATCAGGGGAAACCAAGATATCCGAAGGAGCCTAGAGAGATCAGGCCAGGAATGA**AGGT**
VDR1
CACAGATCTCCATCCAGCAGGCTCTTTACTCCTTCCCTTCCCTACCCCCGCCTCTTTCCCTTTCTTTCTCT
AR 1 AR 4
TTCCTTCATTTTTACT**TGTCTGGTTGTGCTT**TCCTTTTCCATTTCTTATTT**TTTCTTTCTCTTCTC**TATTCTTG

ACTTTCCTCCTCGTCCATTTCTTTCCATTGCTCATTTAGTAAAACTGCGTCCGTGCAGATTTCCCCGTGAG

CCGCCTCGCCGGCTTCACTTAGGAGTGCATGCGCCTGTATGAGTGCGTGTGTCTGTGCGGGGCAAACCC

TGCGGAGAGGCGAGGGCAGCGCGTGTGCACGTGTGAGTGTGCCTGTGAGAGTGTGCGCACAGGAGTGT

GCTCTTGTATGCACGCGTAAAGGGGACTGTGTATGTCGGCGTTGAAGTGTGACTGTGGAATGTGCGCGC

GTGTGTGACTGGCGTGTATGAGTGAATCTGTGTCAGTTGGTGTGAGAGTGTGCACACGCC**TGTGTGAGT**
AR 3
GTCCCTGTGTGAGCACGCGTGTGTTCGAGTGCCCACTCCTCCCC**GCGCTGCAAAGTGCA**GGGGGCGGG
VDR4
CCGGGCGGCAGGGGGCCTGCCCGCTGGATTCCCGCATGCTTGTTCCG**GGGCGGTCGGGTCTA**AAGGG
VDR2
CTTTATGCACTGTCTGGAGGGTGGGGACTGGCGCGGGTAGAAAACGGGATGCCTCGGGCGTGGGGGCA

GGCTTTTGGCCACTAGGAGCTGGCGGAGGTGCAGACCTAAAGGAGCGTTCGCTAGCAGAGGCGCTGCC

GGTGCGGTGTGCTACGCGCGCCCACCTCCCGGGGA**AGGAACG**GCGAGGCC**GGGGACCGT**CGCGGAG
AR 2 VDR3
ATGGATCGCGGGCCGGCAGCAGTGGCGTGCACGCTGCTCCTGGCTCTCGTCGCCTGCCTAGCGCCGGC

CAGTGGCCAAGGTAAGAGCCCAGCCAGAG-3'

B.

Motif ID	P-Value	Matched Sequence
RXRA::VDR 1	0.000307	AGGTCACAGATCTCC
RXRA::VDR 2	0.002520	GGGCGGTCGGGTCTA
RXRA::VDR 3	0.006550	CGGTCCCCGGCCTCG
RXRA::VDR 4	0.006940	GCGCTGCAAAGTGCA
AR 1	0.000211	AAGCACAACCAGACA
AR 2	0.000390	AGGAACGGCGAGGCC
AR 3	0.000626	AGGGACACTCACACA
AR 4	0.000778	GAGAAGAGAAAGAAA

Figure S2. Vitamin D receptor and androgen receptor response elements in LRP2 promoter. A, -791 bp of LRP2 promoter showing mapped areas for VDR and AR response elements. **B,** Jasper prediction of the binding sites with P-value. Note that VDR binds VDREs as an obligate heterodimer with RXRα.

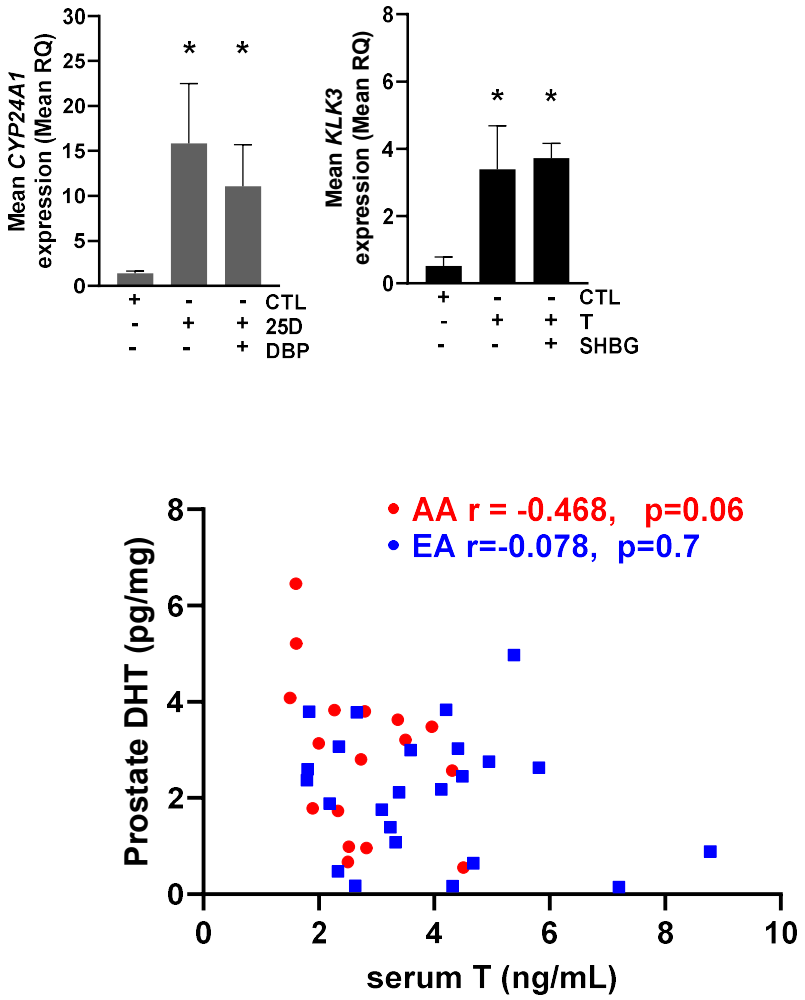

Figure S3. *Lrp2* is regulated by androgens in mouse prostate. scRNAseq data for *Lrp2* expression in mouse prostate epithelial cells following castration and regeneration with testosterone add back. Data from Karthaus et al 2020.

Table S1. Cell and tissue characteristics

MODEL	TISSUE	MORPHOLOGY	DISEASE	ETHINICITY
PrE-AA1	Prostate	Epithelial	Benign	African American
PrE-AA2	Prostate	Epithelial	Benign	African American
957E-hTERT	Prostate	Epithelial	Cancer (local)	Unknown
HEK293	Kidney	Epithelial	Benign	Unknown
LNCaP	Prostate	Epithelial	Cancer (lymph node)	Unknown
TS-AA1	Prostate	Epithelial	Benign	African American
TS-H1	Prostate	Epithelial	Benign	Hispanic

Table S2. Primer sequences

SPECIES	GENE	FORWARD (5' -> 3')	REVERSE (5' -> 3')
HUMAN	***LRP2***	CTCCTGGGTGTGTGACCAA	CATCGGGGCAGTCTCTGAC
	KLK3	TCCAATGACGTGTGTGCGCA	CCTTGATCCACTTCCGGTAA
	CYP24A1	GGCAACAGTTCTGGGTGAAT	ATTTGAGGACAATCCAACA
	CYP27B1	TTTGCATCTCTTCCCTTTGG	CTCAGGCTGCACCTCAAAAT
	VDR	GACCTGTGGCAACCAAGACT	GAACTTGATGAGGGGCTCAA
	SRD5A2	ATATATTGCGCCAGCTCAGG	GGAAATTGGCTCCAGAAACA
	AR	TTGTGTCAAAAGCGAAATGG	CAATGGGCAAAACATGGTC
	RPL13A	GGATAAGAAACCCTGCGACA	CTCGACCATCAAGCACCAG
	HPRT	TGCTGACCTGCTGGATTACA	CTGCATTGTTTTGCCAGTGT
MOUSE	***Pb-MerCreMer*-mutant (genotyping)**	ACGACCAAGTGACAGCAATG	TAAGCAATCCCCAGAAATGC
	***Pb-MerCreMer*-wild type (genotyping)**	CTAGGCCACAGAATTGAAAGATCT	GTAGGTGGAAATTCTAGCATCATC
	Lrp2-Flox* (genotyping, *wt = 206bp, flox=320bp)	CACCATGTCCCTCAGTTGTG	CACCATGTCCCTCAGTTGTG
	***Lrp2 exons 71-75* (recombination)**	CACCGTTGAGTGTGATGCAG	CACCGATGTCCATGTTCACA
	***Lrp2 exons 76-77* (control)**	CTGGTTTTCCACATTTTCTGG	CTGGTTTTCCACATTTTCTGG